







## Article

# Ellagic Acid and Its Metabolites as Potent and Selective Allosteric Inhibitors of Liver Pyruvate Kinase

Umberto Maria Battisti <sup>1,2,†</sup>, Chunixa Gao <sup>1,2,†</sup>, Fady Akladios <sup>1,2</sup>, Woonghee Kim <sup>2</sup>, Hong Yang <sup>2</sup>, Cemil Bayram <sup>3</sup>, Ismail Bolat <sup>4</sup>, Metin Kiliclioglu <sup>4</sup>, Nursena Yuksel <sup>5</sup>, Ozlem Ozdemir Tozlu <sup>5</sup>, Cheng Zhang <sup>2,6</sup>, Jihad Sebhaoui <sup>7</sup>, Shazia Iqbal <sup>7</sup>, Saeed Shoaei <sup>2,8</sup>, Ahmet Hacimuftuoglu <sup>3</sup>, Serkan Yildirim <sup>4</sup>, Hasan Turkez <sup>9</sup>, Mathias Uhlen <sup>2</sup>, Jan Boren <sup>10,11</sup>, Adil Mardinoglu <sup>2,8</sup> and Morten Grøtli <sup>1,\*</sup>

<sup>1</sup> Department of Chemistry and Molecular Biology, University of Gothenburg, 412 96 Gothenburg, Sweden

<sup>2</sup> Science for Life Laboratory, KTH–Royal Institute of Technology, 104 50 Stockholm, Sweden

<sup>3</sup> Department of Medical Pharmacology, Faculty of Medicine, Atatürk University, Erzurum 25240, Turkey

<sup>4</sup> Department of Pathology, Faculty of Veterinary, Atatürk University, Erzurum 25240, Turkey

<sup>5</sup> Department of Molecular Biology and Genetics, Faculty of Science, Erzurum Technical University, Erzurum 25050, Turkey

<sup>6</sup> School of Pharmaceutical Sciences, Zhengzhou University, Zhengzhou 450001, China

<sup>7</sup> Trustlife Labs, Drug Research & Development Center, Istanbul 34774, Turkey

<sup>8</sup> Centre for Host-Microbiome Interactions, Faculty of Dentistry, Oral & Craniofacial Sciences, King's College London, London SE1 9RT, UK

<sup>9</sup> Department of Medical Biology, Faculty of Medicine, Atatürk University, Erzurum 25240, Turkey

<sup>10</sup> Department of Molecular and Clinical Medicine, University of Gothenburg, 405 30 Gothenburg, Sweden

<sup>11</sup> Sahlgrenska University Hospital, 405 30 Gothenburg, Sweden

\* Correspondence: grotli@chem.gu.se; Tel.: +46-766229017

† These authors contributed equally to this work.



**Citation:** Battisti, U.M.; Gao, C.; Akladios, F.; Kim, W.; Yang, H.; Bayram, C.; Bolat, I.; Kiliclioglu, M.; Yuksel, N.; Tozlu, O.O.; et al. Ellagic Acid and Its Metabolites as Potent and Selective Allosteric Inhibitors of Liver Pyruvate Kinase. *Nutrients* **2023**, *15*, 577. <https://doi.org/10.3390/nu15030577>

Academic Editor: Lynnette Ferguson

Received: 14 December 2022

Revised: 14 January 2023

Accepted: 18 January 2023

Published: 22 January 2023



**Copyright:** © 2023 by the authors. Licensee MDPI, Basel, Switzerland. This article is an open access article distributed under the terms and conditions of the Creative Commons Attribution (CC BY) license (<https://creativecommons.org/licenses/by/4.0/>).

**Abstract:** Liver pyruvate kinase (PKL) has recently emerged as a new target for non-alcoholic fatty liver disease (NAFLD), and inhibitors of this enzyme could represent a new therapeutic option. However, this breakthrough is complicated by selectivity issues since pyruvate kinase exists in four different isoforms. In this work, we report that ellagic acid (EA) and its derivatives, present in numerous fruits and vegetables, can inhibit PKL potently and selectively. Several polyphenolic analogues of EA were synthesized and tested to identify the chemical features responsible for the desired activity. Molecular modelling studies suggested that this inhibition is related to the stabilization of the PKL inactive state. This unique inhibition mechanism could potentially herald the development of new therapeutics for NAFLD.

**Keywords:** NAFLD; liver pyruvate kinase; ellagic acid; urolithins; enzyme inhibition

## 1. Introduction

In the past decades, lifestyle modifications have drastically affected health priorities in several areas of the world, and emerging pathologies have changed the medical landscape. Non-alcoholic fatty liver disease (NAFLD) is a new chronic liver disease and is strongly associated with the worldwide increase in obesity [1]. NAFLD is an umbrella term that includes several liver abnormalities such as excess triglyceride accumulation, ballooning degeneration, inflammation, fibrosis, and cirrhosis [2]. Almost 33% of adults in the U.S. are affected by hepatic steatosis, even though this number might be even higher [3]. It is estimated that 15–20% of these individuals will develop non-alcoholic steatohepatitis, with 15–20% of these further progressing to cirrhosis [4]. Due to these alarming data, NAFLD has been recognized as an important cause of liver disease, and will likely grow into the leading cause of end-stage liver disease within the next decade. Despite the alarming prevalence of NAFLD, no therapy has yet been approved; the only available option has been weight loss (e.g., calorie restriction, exercise, etc.), and possibly vitamin

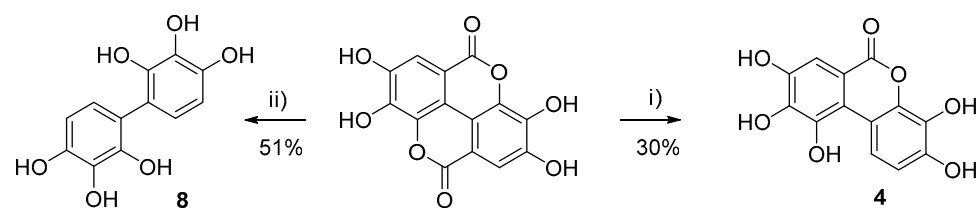
E supplementation [5]. Therefore, it is crucial to discover and validate novel biomarkers and drug targets for the early diagnosis and effective treatment of NAFLD [6]. We recently employed an innovative approach based on integrative network analyses to identify new targets for NAFLD treatment with minimal side effects [7]. This study suggested that downregulation and/or an inhibition of liver pyruvate kinase (PKL) could serve as a successful strategy to block and even reverse NAFLD progression. Krishnan et al. reached a similar conclusion employing *in vivo* and *in vitro* knock-out models [8]. PKL has also been identified as one of the driver genes responsible for NAFLD, and is therefore a key target for the development of treatment strategies [9].

Pyruvate kinase (PK) is an enzyme that catalyzes the final step in glycolysis, converting phosphoenolpyruvate (PEP) and adenosine diphosphate (ADP) to pyruvate (PYR) and adenosine triphosphate (ATP). There are four mammalian pyruvate kinase isoforms, PKM1, PKM2, PKR, and PKL, and each isoform has had multiple designations over time in the literature [10]. Although a tissue may express more than one pyruvate kinase isoform, individual cells generally express only one at appreciable levels. Most adult tissues express PKM2, and expression of the other three isoforms is restricted to distinct tissues and cell types [11–13]. The PKL isoform is expressed in the liver, pancreatic  $\beta$ -cells, small intestine, and renal proximal tubule [14]. PKL inhibitors may be useful in halting NAFLD progression [7], but potent and selective inhibitors have not been reported in the literature. However, it is well known that some natural molecules, in particular polyphenolic compounds, potently inhibit the PKM2 isoform [15–17]. Most of these polyphenols have been found to possess a variety of pharmacological effects on oxidative stress, lipid metabolism, insulin resistance, and inflammation, which are all important pathological processes in the etiology of liver diseases such as NAFLD [18–21]. The mechanisms underlying the beneficial effects of many polyphenols on NAFLD have been extensively studied in recent years. In addition to the indirect antioxidant and anti-inflammatory effects and regulation of classical intracellular signal transduction, it has been demonstrated that some polyphenols exert their therapeutic effects through emerging new mechanisms (e.g., reduction of *de novo* lipogenesis and increased fatty acid  $\beta$ -oxidation) [18]. For these reasons, we hypothesized that some polyphenols might be beneficial in NAFLD due to PKL inhibition. EA is a naturally occurring polyphenolic compound found in numerous fruits, nuts, and seeds, such as pomegranates, grapes, raspberries, and walnuts, with antioxidative, anti-obesity, hypolipidemic, and antidiabetic effects [22]. Furthermore, EA has been reported to be an ATP competitive inhibitor of protein kinase CK2 [23]. Therefore, we aimed to test EA and urolithins, EA's metabolites, to evaluate their inhibitory activity against PKL.

## 2. Materials and Methods

### 2.1. Materials

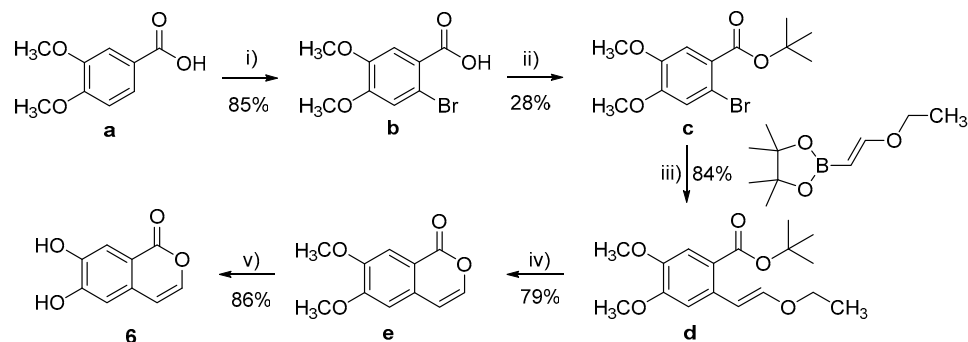
Compounds 1–3 and 7 were purchased from Sigma-Aldrich, Stockholm, Sweden while compounds 5, 11, and 12 were purchased from Toronto Research Chemicals (20 Martin Ross Avenue, North York, M3J 2K8, Toronto, ON, Canada). All other target molecules (4, 6, 8–10, and 13–15) were synthesized in-house (Schemes 1–5).



**Scheme 1.** Synthesis of 4 and 8 from ellagic acid. Reagents and conditions: (i) KOH, H<sub>2</sub>O, 100 °C, 2 h; (ii) KOH, H<sub>2</sub>O, 170 °C, 2 h.

3,4,8,9,10-Pentahydroxy-6H-benzo[c]chromen-6-one (4)

The compound was synthesized according to the literature procedure [24]. A solution of ellagic acid (0.100 g, 0.33 mmol) in aqueous KOH (0.8 g, 5.0 mL) was heated at 100 °C for 20 min. The mixture was then cooled to rt and acidified (pH 1). The aqueous phase was extracted with Et<sub>2</sub>O (3 × 20 mL). The combined organic layers were dried (Na<sub>2</sub>SO<sub>4</sub>), filtered, and concentrated to give a yellow powder. The solid obtained was recrystallized from water to give 0.025 g (30%) of the target compound as a grey solid. m.p. = 230–232 °C, <sup>1</sup>H-NMR (CD<sub>3</sub>OD, 400 MHz): 6.75 (d, J = 9.0 Hz, 1H, Ar-H), 7.37 (s, 1H, Ar-H), 8.44 (d, J = 9.0 Hz, 1H, Ar-H); <sup>13</sup>C-NMR (CD<sub>3</sub>OD, 100 MHz): 106.6, 110.7, 111.0, 111.4, 117.1, 117.7, 131.9, 139.6, 140.3, 142.6, 145.0, 145.4, 162.3; HRMS: found M-H: m/z 275.0206, calculated value for C<sub>13</sub>H<sub>7</sub>O<sub>7</sub><sup>-</sup>: 275.0197 (delta: −3.3 ppm).



**Scheme 2.** Synthesis of 6. Reagents and conditions: (i) Br<sub>2</sub>, HCl, rt, 2 h; (ii) *t*-BuOH, MgSO<sub>4</sub>, H<sub>2</sub>SO<sub>4</sub>, CH<sub>2</sub>Cl<sub>2</sub>, rt, 48 h; (iii) Na<sub>2</sub>CO<sub>3</sub>, Pd(PPh<sub>3</sub>)<sub>3</sub>, H<sub>2</sub>O, Dioxane, 110 °C, 2 h; (iv) TFA, 100 °C, 2 h; (v) BBr<sub>3</sub>, CH<sub>2</sub>Cl<sub>2</sub>, rt, 12 h.

#### 2-Bromo-4,5-Dimethoxybenzoic Acid (b)

The compound was synthesized according to the literature procedure [25]. To a suspension of 3,4-dimethoxybenzoic acid (a, 5.00 g, 27.44 mmol) in HCl conc. (100 mL), bromine (4.82 g, 30.19 mmol) was added dropwise at rt. The reaction mixture was stirred for 2 h at rt. Water (100 mL) was then added, and the resulting precipitate was collected by filtration, and recrystallized from MeOH to give 6.1 g (85%) of 2-bromo-3,4-dimethoxybenzoic acid as a white solid. m.p. = 185–187 °C, <sup>1</sup>H-NMR (DMSO-*d*<sub>6</sub>, 400 MHz): 3.76 (s, 3H, CH<sub>3</sub>), 3.81 (s, 3H, CH<sub>3</sub>), 7.16–7.20 (m, 1H, Ar-H), 7.31–7.37 (m, 1H, Ar-H); <sup>13</sup>C-NMR (DMSO-*d*<sub>6</sub>, 100 MHz): 56.1, 56.2, 112.8, 114.2, 124.4, 148.0, 151.9, 166.9.

#### *tert*-Butyl 2-bromo-4,5-dimethoxybenzoate (c)

The compound was synthesized according to the literature procedure [26]. To a solution of 2-bromo-3,4-dimethoxybenzoic acid (b, 1.30 g, 5.00 mmol) in CH<sub>2</sub>Cl<sub>2</sub>, MgSO<sub>4</sub> (2.41 g, 20 mmol) was added. The flask was then purged with nitrogen and H<sub>2</sub>SO<sub>4</sub> (0.46 g, 4.75 mmol) and *tert*-butanol (1.85 g, 25.00 mmol) was added. The reaction was stirred at rt for 48 h. The reaction was quenched by addition of EtOAc/pentane (20 mL, 50/50), followed by saturated NaHCO<sub>3</sub> solution. The layers were separated, and the organic layer was dried (Na<sub>2</sub>SO<sub>4</sub>), filtered, and concentrated in vacuum. The crude mixture was purified by flash chromatography (90/10 pentane/EtOAc) to give 0.41 g (26%) of *tert*-butyl 2-bromo-4,5-dimethoxybenzoate as a colorless oil. <sup>1</sup>H-NMR (CDCl<sub>3</sub>, 400 MHz) = 1.56 (s, 9H, 3 × CH<sub>3</sub>), 3.84 (s, 3H, CH<sub>3</sub>), 3.86 (s, 3H, CH<sub>3</sub>), 7.00 (s, 1H, Ar-H), 7.27 (s, 1H, Ar-H); <sup>13</sup>C-NMR (CDCl<sub>3</sub>, 400 MHz) = 28.1, 56.0, 56.2, 82.2, 113.1, 113.8, 116.6, 125.2, 147.7, 151.4, 165.0.

#### (*E*)-*tert*-Butyl 2-(2-ethoxyvinyl)-4,5-dimethoxybenzoate (d)

The compound was synthesized according to the literature procedure [27]. *tert*-Butyl 2-bromo-4,5-dimethoxybenzoate (0.10 g, 0.31 mmol), *trans*-2-ethoxyvinylboronic acid pinacol ester (0.06 g, 0.31 mmol), palladium tetrakis (0.072 g, 0.06 mmol), and sodium carbonate (0.10 g, 0.94 mmol) were placed in a 5.0 mL microwave vial. A degassed solution of dioxane/water (50:50, 4 mL) was added. The mixture was stirred for 2 h at 110 °C in

the microwave. The solution was then rinsed with water (20.0 mL) and extracted with EtOAc (3 × 20.0 mL). The organic phase was dried (Na<sub>2</sub>SO<sub>4</sub>), filtered, and concentrated in vacuum to give 0.12 g of crude product. Purification by flash chromatography (90/10 pentane/EtOAc) afforded 0.070 g (72%) of the target compound as a yellow oil. <sup>1</sup>H-NMR (CDCl<sub>3</sub>, 400 MHz): 1.34 (t, J = 7.03, 3H, CH<sub>3</sub>), 1.58 (s, 9H, C(CH<sub>3</sub>)<sub>3</sub>), 3.84–3.96 (m, 8H, CH<sub>2</sub>, 2 × CH<sub>3</sub>), 6.69 (d, J = 12.9 Hz, 1H, CH), 6.78 (s, 1H, Ar-H), 6.81 (d, J = 12.9 Hz, 1H, CH), 7.38 (s, 1H, Ar-H); <sup>13</sup>C-NMR (CDCl<sub>3</sub>, 100 MHz): 14.8, 28.3, 55.8, 55.9, 65.1, 80.8, 105.4, 108.6, 113.5, 121.4, 132.1, 146.7, 148.2, 151.5, 166.6.

#### 6,7-Dimethoxy-1H-isochromen-1-one (e)

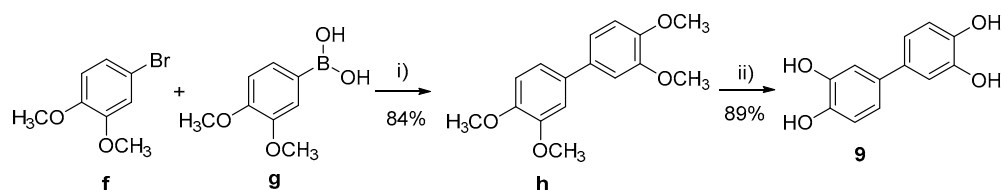
The compound was synthesized according to the literature procedure [27]. A solution of (E)-*tert*-butyl 2-(2-ethoxyvinyl)-4,5-dimethoxybenzoate (0.640 g, 2.07 mmol) in TFA (14.0 mL) in a sealed microwave reactor was heated at 100 °C for 2 h under microwaved-assisted conditions. The reaction mixture was evaporated to dryness. The residue was purified by flash chromatography (70/30 pentane/EtOAc) to give 0.34 g (79%) of the target compound as a yellow solid. m.p. = 116–118 °C; <sup>1</sup>H-NMR (CDCl<sub>3</sub>, 400 MHz): 3.88 (s, 3H, CH<sub>3</sub>), 3.91 (s, 3H, CH<sub>3</sub>), 6.35 (d, J = 5.6 Hz, 1H, CH), 6.72 (s, 1H, Ar-H), 7.15 (d, J = 5.6 Hz, 1H, CH), 7.53 (s, 1H, Ar-H); <sup>13</sup>C-NMR (CDCl<sub>3</sub>, 100 MHz): 56.1, 56.2, 106.2, 106.6, 109.3, 114.8, 132.0, 143.7, 149.7, 155.0, 162.1.

#### 6,7-dihydroxy-1H-isochromen-1-one (6)

To a solution of 6,7-dimethoxy-1H-isochromen-1-one (0.270 g, 1.31 mmol) in CH<sub>2</sub>Cl<sub>2</sub> (30.0 mL), BBr<sub>3</sub> in CH<sub>2</sub>Cl<sub>2</sub> (1.0 M, 5.76 mmol) was added dropwise at 0 °C. The solution was stirred at rt for 2 h. Water (20.0 mL) was added to quench the reaction and CH<sub>2</sub>Cl<sub>2</sub> was removed under vacuum. The aqueous layer was extracted with ethyl acetate (3 × 20.0 mL). The combined organic phase was dried (Na<sub>2</sub>SO<sub>4</sub>), filtered, and concentrated in vacuum. The solid obtained was triturated in pentane and filtered to afford 0.200 g (86%) of the target compound, as a dark brown solid. m.p. = 265–267 °C; <sup>1</sup>H-NMR (DMSO-*d*<sub>6</sub>, 400 MHz): 6.57 (d, J = 5.6 Hz, 1H, CH), 6.88 (s, 1H, Ar-H), 7.34 (d, J = 5.6 Hz, 1H, CH), 7.42 (s, 1H, Ar-H), 9.96 (br s, 1H, OH), 10.40 (br s, 1H, Ar-H); <sup>13</sup>C-NMR (DMSO-*d*<sub>6</sub>, 100 MHz): 106.9, 111.1, 113.5, 113.6, 131.1, 143.7, 147.3, 153.5, 161.7; HRMS: found M-H: m/z 177.0198, calculated value for C<sub>9</sub>H<sub>6</sub>O<sub>4</sub><sup>-</sup>: 177.0193 (delta: −2.8 ppm).

#### [1,1'-Biphenyl]-2,2',3,3',4,4'-hexaol (8)

The compound was synthesized according to the literature procedure [24]. A solution of ellagic acid (0.500 g, 1.65 mmol) in aqueous NaOH (5 M, 5.0 mL) was heated at 170 °C for 2 h. The mixture was then cooled to rt and acidified (pH 1). The solid obtained was filtered and recrystallized from water to give 0.21 g (51%) of [1,1'-biphenyl]-2,2',3,3',4,4'-hexaol as a brown solid. m.p. >350 °C, <sup>1</sup>H-NMR (DMSO-*d*<sub>6</sub>, 400 MHz): 6.32 (d, J = 8.4 Hz, 2H, Ar-H), 6.40 (d, J = 8.4 Hz, 2H, Ar-H); <sup>13</sup>C-NMR (DMSO-*d*<sub>6</sub>, 100 MHz): 107.8, 119.0, 121.0, 133.7, 143.4, 145.3; HRMS: found M-H: m/z 249.0411, calculated value for C<sub>12</sub>H<sub>9</sub>O<sub>6</sub><sup>-</sup>: 249.0405 (delta: 2.1 ppm).



**Scheme 3.** Synthesis of 9. Reagents and conditions: (i) Na<sub>2</sub>CO<sub>3</sub>, Pd(PPh<sub>3</sub>)<sub>3</sub>, H<sub>2</sub>O, Dioxane, 110 °C, 2 h; (ii) BBr<sub>3</sub>, CH<sub>2</sub>Cl<sub>2</sub>, rt, 12 h.

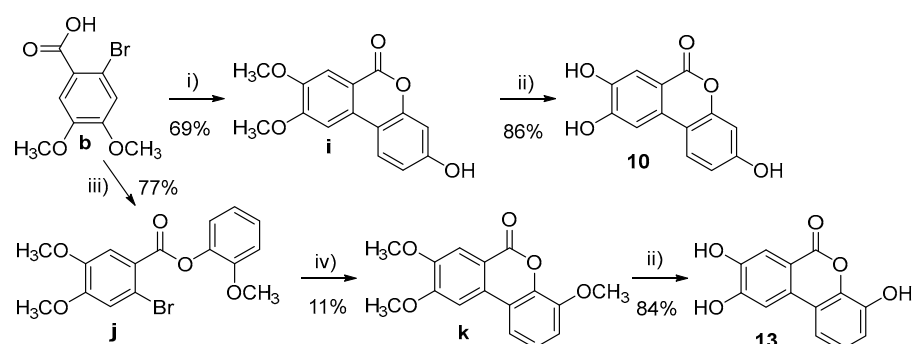
#### 3,3',4,4'-tetramethoxy-1,1'-biphenyl (h)

The compound was synthesized according to the literature procedure [28]. 4-Bromove-ratrole (f, 0.50 g, 2.30 mmol), 3,4-dimethoxybenzeneboronic acid (g, 0.46 g, 2.53 mmol),

palladium tetrakis (0.27 g, 0.23 mmol), and potassium carbonate (1.27 g, 9.20 mmol) were placed in a 20.0 mL microwave vial. A degassed solution of dioxane/water (50:50, 12.0 mL) was added. The mixture was stirred for 1 h at 110 °C in the microwave. The solution was then rinsed with water (20.0 mL) and extracted with EtOAc (3 × 20.0 mL). The organic phase was dried (Na<sub>2</sub>SO<sub>4</sub>), filtered, and concentrated in a vacuum to give 0.7 g of crude product. Purification by flash chromatography (70/30 pentane/EtOAc) afforded 0.53 g (84%) of the target compound as a white solid. m.p. = 133–135 °C, <sup>1</sup>H-NMR (CDCl<sub>3</sub>, 400 MHz): 3.85 (s, 6H, CH<sub>3</sub>), 3.89 (s, 6H, CH<sub>3</sub>), 6.86 (d, 2H, J = 8.1 Hz, Ar-H), 7.02–7.07 (m, 4H, Ar-H); <sup>13</sup>C-NMR (CDCl<sub>3</sub>, 100 MHz): 55.9, 110.3, 111.5, 119.2, 134.1, 148.3, 149.1.

#### [1,1'-biphenyl]-3,3',4,4'-tetraol (**9**)

The compound was synthesized according to the literature procedure [29]. To a solution of 3,3',4,4'-tetramethoxy-1,1'-biphenyl (**h**, 0.415 g, 1.51 mmol) in CH<sub>2</sub>Cl<sub>2</sub> (30.0 mL), BBr<sub>3</sub> in CH<sub>2</sub>Cl<sub>2</sub> (1.0 M, 18.15 mmol) was added dropwise at 0 °C. The solution was stirred at rt for 2 h. Water was added to quench the reaction and CH<sub>2</sub>Cl<sub>2</sub> was removed under vacuum. The aqueous layer was extracted with ethyl acetate (3 × 30 mL). The combined organic phase was dried (Na<sub>2</sub>SO<sub>4</sub>), filtered, and concentrated in vacuum. The solid obtained was triturated in pentane and filtered to afford 0.29 g (89%) of the target compound as a white solid. m.p. = 232–234 °C; <sup>1</sup>H-NMR (CD<sub>3</sub>OD, 400 MHz): 6.76 (d, J = 8.2 Hz, 2H, Ar-H), 6.83 (dd, J = 2.2, 8.2 Hz, 2H, Ar-H), 144.9; HRMS: found M-H: m/z 217.0514, calculated value for C<sub>12</sub>H<sub>9</sub>O<sub>4</sub>: 217.0506 (delta: −3.7 ppm).



**Scheme 4.** Synthesis of **10** and **13**. Reagents and conditions: (i) NaOH, Na<sub>2</sub>CO<sub>3</sub>, resorcinol, CuI, H<sub>2</sub>O, 50 °C, 12 h; (ii) BBr<sub>3</sub>, CH<sub>2</sub>Cl<sub>2</sub>, rt, 12 h; (iii) SOCl<sub>2</sub>, reflux, 2 h, then Et<sub>3</sub>N, 2-methoxyphenol, CH<sub>2</sub>Cl<sub>2</sub>, rt, 12 h; (iv) NaOAc, Cy<sub>3</sub>P·HBF<sub>4</sub>, Pd(OAc)<sub>2</sub>, DMF, reflux, 72 h.

#### 3-Hydroxy-8,9-dimethoxy-6H-benzo[c]chromen-6-one (**i**)

The compound was synthesized according to the literature procedure [30]. To a suspension of 2-bromo-3,4-dimethoxybenzoic acid (**b**, 1.04 g, 4.00 mmol) and resorcinol (1.32 g, 12.00 mmol) in H<sub>2</sub>O (10.0 mL), NaOH solution (4 M, 1.0 mL) was added. The solution was stirred at rt until complete dissolution and subsequently Na<sub>2</sub>CO<sub>3</sub> (0.93 g, 8.80 mmol) was added. The mixture was stirred at 50 °C for 10 min and then CuI (0.23 g, 1.20 mmol) was added. The resulting suspension was stirred at 50 °C for 12 h. The precipitate formed was filtered, washed with CH<sub>3</sub>OH, dried and triturated with Et<sub>2</sub>O to give 0.75 g (69%) of the target compound as a white solid. m.p. = 329–331 °C; <sup>1</sup>H-NMR (DMSO-*d*<sub>6</sub>, 400 MHz): 3.85 (s, 3H, CH<sub>3</sub>), 3.98 (s, 3H, CH<sub>3</sub>), 6.60–6.93 (m, 2H, Ar-H), 7.41–7.69 (m, 2H, Ar-H), 8.15 (s, 1H, Ar-H), 10.19 (br s, 1H, OH); <sup>13</sup>C-NMR (DMSO-*d*<sub>6</sub>, 100 MHz): 56.0, 56.6, 103.1, 103.7, 109.9, 112.0, 113.2, 125.0, 130.7, 149.2, 152.1, 155.5, 159.4, 160.7.

#### 3,8,9-trihydroxy-6H-benzo[c]chromen-6-one (**10**)

To a solution of 3-hydroxy-8,9-dimethoxy-6H-benzo[c]chromen-6-one (**i**, 0.100 g, 0.37 mmol) in CH<sub>2</sub>Cl<sub>2</sub> (10.0 mL), BBr<sub>3</sub> in CH<sub>2</sub>Cl<sub>2</sub> (1.0 M, 2.42 mmol) was added dropwise at 0 °C. The solution was stirred at rt for 48 h. MeOH was added to quench the reaction and the solvent was removed under vacuum. The solid obtained was triturated in Et<sub>2</sub>O and filtered to afford 0.076 g (85%) of the target compound as a white solid. m.p. > 350 °C;

$^1\text{H-NMR}$  (DMSO- $d_6$ , 400 MHz): 6.62 (d,  $J = 2.0$  Hz, 1H, Ar-H), 6.75 (dd,  $J = 2.0, 8.6$  Hz, 1H, Ar-H), 7.39 (s, 1H, Ar-H), 7.45 (s, 1H, Ar-H), 7.80 (d,  $J = 8.6$  Hz, 1H, Ar-H), 10.17 (br s, 3H, OH);  $^{13}\text{C-NMR}$  (DMSO- $d_6$ , 100 MHz): 103.2, 107.3, 110.2, 111.3, 113.3, 114.6, 124.1, 129.6, 146.5, 151.9, 153.8, 159.0, 160.7; HRMS: found M-H:  $m/z$  243.0306, calculated value for  $\text{C}_{13}\text{H}_7\text{O}_5$ : 243.0299 ( $\delta$ :  $-2.9$  ppm).

#### 2-Methoxyphenyl 2-bromo-4,5-dimethoxybenzoate (j)

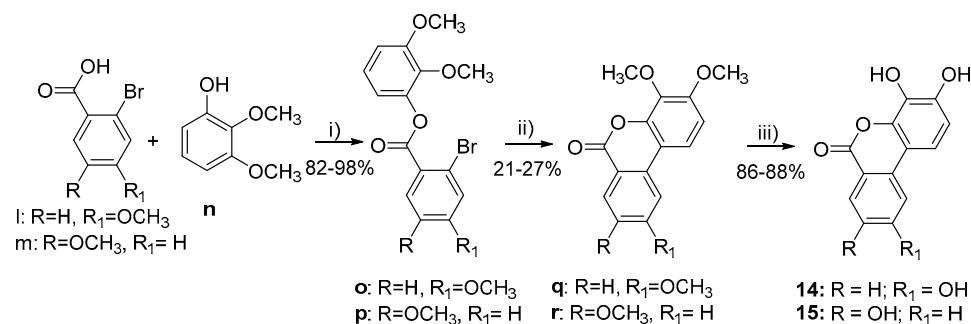
A solution of 2-bromo-3,4-dimethoxybenzoic acid (**b**, 1.30 g, 4.33 mmol) in thionyl chloride (10.0 mL) was refluxed for 2 h, and then the solvent was removed in vacuo. The oil obtained was solubilized in  $\text{CH}_2\text{Cl}_2$  (10 mL), and added dropwise to a solution of 2-methoxyphenol (0.680 g, 5.48 mmol) and Et<sub>3</sub>N (0.75 g, 7.47 mmol) in  $\text{CH}_2\text{Cl}_2$  (10.0 mL). The mixture was stirred at rt for 2 h and concentrated in vacuo. Purification by flash chromatography (80/20 Hexane/EtOAc) afforded 1.41 g (77%) of 2-methoxyphenyl 2-bromo-4,5-dimethoxybenzoate as a colorless oil.  $^1\text{H-NMR}$  ( $\text{CDCl}_3$ , 400 MHz): 3.84 (s, 3H, CH<sub>3</sub>), 3.94 (s, 3H, CH<sub>3</sub>), 3.95 (s, 3H, CH<sub>3</sub>), 6.95–7.04 (m, 2H, Ar-H), 7.15–7.20 (m, 2H, Ar-H), 7.21–7.27 (m, 1H, Ar-H), 7.68 (s, 1H, Ar-H);  $^{13}\text{C-NMR}$  ( $\text{CDCl}_3$ , 100 MHz): 55.9, 56.2, 56.3, 112.5, 114.5, 115.3, 117.1, 120.8, 121.9, 123.0, 127.0, 139.8, 147.8, 151.2, 152.5, 163.2.

#### 4,8,9-Trimethoxy-6H-benzo[*c*]chromen-6-one (k)

To a solution of 2-methoxyphenyl 2-bromo-4,5-dimethoxybenzoate (1.30 g, 3.54 mmol) in dry DMF (10.0 mL), NaOAc (0.58 g, 7.08 mmol), Pd(OAc)<sub>2</sub> (0.07 g, 0.35 mmol), and tricyclohexylphosphine tetrafluoroborate (0.39 g, 1.06 mmol) were added. The mixture was degassed and then refluxed under nitrogen for 3 days. The reaction mixture was cooled to rt, and then diluted with diethyl ether and filtered through Celite to remove the catalyst. The solvent was removed under vacuum to give 1.1 g of a dark oil. Crystallization from MeOH afforded 0.11 g (11%) of the target compound as a white solid. m.p. = 222–224 °C;  $^1\text{H-NMR}$  (DMSO- $d_6$ , 400 MHz): 3.89 (s, 3H, CH<sub>3</sub>), 3.90 (s, 3H, CH<sub>3</sub>), 4.01 (s, 3H, CH<sub>3</sub>), 7.17 (dd,  $J = 1.3, 8.2$  Hz, 1H, Ar-H), 7.29 (app t,  $J = 8.1$  Hz, 1H, Ar-H), 7.57 (s, 1H, Ar-H), 7.75 (s, 1H, Ar-H), 7.90 (dd,  $J = 1.3, 8.3$  Hz, 1H, Ar-H);  $^{13}\text{C-NMR}$  (DMSO- $d_6$ , 100 MHz): 56.2, 56.4, 56.8, 105.0, 110.1, 112.4, 113.8, 115.2, 118.9, 124.6, 130.1, 140.2, 147.6, 150.4, 155.5, 160.0.

#### 4,8,9-Trihydroxy-6H-benzo[*c*]chromen-6-one (13)

To a solution of 4,8,9-trimethoxy-6H-benzo[*c*]chromen-6-one (0.07 g, 0.24 mmol) in  $\text{CH}_2\text{Cl}_2$  (20 mL), BBr<sub>3</sub> in  $\text{CH}_2\text{Cl}_2$  (1.0 M, 2.20 mmol) was added dropwise at 0 °C. The solution was stirred at rt for 12 h. Water (20 mL) was added to quench the reaction and the aqueous layer was extracted with EtOAc (3 × 20 mL). The organic phase was dried (Na<sub>2</sub>SO<sub>4</sub>), filtered, and concentrated in vacuo to give a brown solid. The solid obtained was triturated in Et<sub>2</sub>O and filtered to afford 0.05 g (84%) of the target compound as a pink powder. m.p. = 345–347 °C;  $^1\text{H-NMR}$  (MeOD, 400 MHz): 6.93 (dd,  $J = 1.4, 8.0$  Hz, 1H, Ar-H), 7.13 (t,  $J = 8.0$  Hz, 1H, Ar-H), 7.45 (dd,  $J = 1.4, 8.0$  Hz, 1H, Ar-H), 7.50 (s, 1H, Ar-H), 7.63 (s, 1H, Ar-H);  $^{13}\text{C-NMR}$  (MeOD, 100 MHz): 107.2, 112.4, 112.8, 114.0, 115.2, 119.1, 124.0, 129.6, 139.3, 145.1, 147.0, 153.3, 161.2; HRMS: found M-H:  $m/z$  243.0308, calculated value for  $\text{C}_{13}\text{H}_7\text{O}_5$ : 243.0299 ( $\delta$ :  $-3.7$  ppm).



**Scheme 5.** Synthesis of 14 and 15. Reagents and conditions: (i)  $\text{SOCl}_2$ , reflux, 2 h, then Et<sub>3</sub>N,  $\text{CH}_2\text{Cl}_2$ , rt, 12 h; (ii) NaOAc,  $\text{Cy}_3\text{P}\cdot\text{HBF}_4$ , Pd(OAc)<sub>2</sub>, DMF, reflux, 72 h; (iii) BBr<sub>3</sub>,  $\text{CH}_2\text{Cl}_2$ , rt, 12 h.

### 2,3-Dimethoxyphenyl 2-bromo-4-methoxybenzoate (**o**)

A solution of 2-bromo-4-methoxybenzoic acid (**l**, 1.0 g, 4.33 mmol) in thionyl chloride (10.0 mL) was refluxed for 2 h, and then the solvent was removed in vacuo. The oil obtained was solubilized in CH<sub>2</sub>Cl<sub>2</sub> (10.0 mL) and added dropwise to a solution of 2,3-dimethoxyphenol (0.73 g, 4.76 mmol), and Et<sub>3</sub>N (0.66 g, 6.49 mmol) in CH<sub>2</sub>Cl<sub>2</sub> (10 mL). The mixture was stirred at rt for 2 h and concentrated in vacuo. Purification by flash chromatography (80/20 Hexane/EtOAc) afforded 1.31 g (82%) of the target compound as a colorless oil. <sup>1</sup>H-NMR (CDCl<sub>3</sub>, 400 MHz): 3.86 (s, 6H, 2 x CH<sub>3</sub>), 3.88 (s, 3H, CH<sub>3</sub>), 6.81 (dd, J = 1.5, 8.2 Hz, 1H, Ar-H), 6.84 (dd, J = 1.5, 8.24 Hz, 1H, Ar-H), 6.93 (dd, J = 2.5, 8.8 Hz, 1H, Ar-H), 7.06 (t, J = 8.3 Hz, 1H, Ar-H), 7.25 (d, J = 2.5 Hz, 1H, Ar-H), 8.13 (d, J = 8.8 Hz, 1H, Ar-H); <sup>13</sup>C-NMR (CDCl<sub>3</sub>, 100 MHz): 55.8, 56.1, 60.9, 110.3, 113.1, 115.3, 120.1, 122.4, 123.5, 124.0, 124.4, 134.0, 141.3, 144.2, 153.8, 162.3, 168.4.

### 3,4,9-Trimethoxy-6H-benzo[*c*]chromen-6-one (**q**)

To a solution of 2,3-dimethoxyphenyl 2-bromo-4-methoxybenzoate (**o**, 1.30 g, 3.54 mmol) in dry DMF (10.0 mL), NaOAc (0.58 g, 7.08 mmol), Pd(OAc)<sub>2</sub> (0.07 g, 0.35 mmol), and tricyclohexylphosphine tetrafluoroborate (0.39 g, 1.06 mmol) were added. The mixture was degassed and then refluxed under nitrogen for 3 days. The reaction mixture was cooled to rt, and then diluted with diethyl ether and filtered through Celite to remove the catalyst. The solvent was under vacuum to give 1.1 g of a dark oil. Crystallization from MeOH afforded 0.270 g (27%) of the target compound as a white solid. m.p. = 183–185 °C; <sup>1</sup>H-NMR (DMSO-*d*<sub>6</sub>, 400 MHz): 3.82 (s, 3H, CH<sub>3</sub>), 3.90 (s, 3H, CH<sub>3</sub>), 3.96 (s, 3H, CH<sub>3</sub>), 7.09 (d, J = 9.1 Hz, 1H, Ar-H), 7.13 (dd, J = 2.4, 8.2 Hz, 1H, Ar-H), 7.71 (d, J = 2.4 Hz, 1H, Ar-H), 8.06–8.12 (m, 2H, Ar-H); <sup>13</sup>C-NMR (DMSO-*d*<sub>6</sub>, 100 MHz): 56.5, 56.7, 61.2, 105.6, 109.4, 112.3, 112.5, 116.7, 119.4, 132.5, 136.2, 137.7, 145.6, 154.5, 160.2, 166.2.

### 3,4,9-Trihydroxy-6H-benzo[*c*]chromen-6-one (**14**)

To a solution of 3,4,9-trimethoxy-6H-benzo[*c*]chromen-6-one (**q**, 0.15 g, 0.52 mmol) in CH<sub>2</sub>Cl<sub>2</sub> (20 mL), BBr<sub>3</sub> in CH<sub>2</sub>Cl<sub>2</sub> (1.0 M, 4.71 mmol) was added dropwise at 0 °C. The solution was stirred at rt for 12 h. Water (20 mL) was added to quench the reaction and the aqueous layer was extracted with EtOAc (3 × 20 mL). The organic phase was dried (Na<sub>2</sub>SO<sub>4</sub>), filtered, and concentrated in vacuo to give a white powder. The solid obtained was triturated in Et<sub>2</sub>O and filtered to afford 0.110 g (86%) of the target compound as a brown solid. m.p. = 301–303 °C; <sup>1</sup>H-NMR (DMSO-*d*<sub>6</sub>, 400 MHz): 6.80 (d, J = 8.7 Hz, 1H, Ar-H), 6.95 (dd, J = 2.2, 8.7 Hz, 1H, Ar-H), 7.40 (d, J = 2.2 Hz, 1H, Ar-H), 7.43 (d, J = 8.8 Hz, 1H, Ar-H), 8.03 (d, J = 8.8 Hz, 1H, Ar-H), 9.19 (br s, 1H, OH), 9.79 (br s, 1H, OH), 10.77 (br s, 1H, OH); <sup>13</sup>C-NMR (DMSO-*d*<sub>6</sub>, 100 MHz): 106.8, 110.6, 110.9, 112.7, 113.7, 116.9, 132.9, 133.1, 138.3, 141.4, 148.4, 160.7, 164.1; HRMS: found M-H: m/z 243.0305, calculated value for C<sub>13</sub>H<sub>7</sub>O<sub>5</sub>: 243.0299 (delta: −2.5 ppm).

### 2,3-Dimethoxyphenyl 2-bromo-5-methoxybenzoate (**p**)

A solution of 2-bromo-5-methoxybenzoic acid (**m**, 1.0 g, 4.33 mmol) in thionyl chloride (10.0 mL) was refluxed for 2 h and then the solvent removed in vacuo. The oil obtained was solubilized in CH<sub>2</sub>Cl<sub>2</sub> (10.0 mL) and added dropwise to a solution of 2,3-dimethoxyphenol (0.73 g, 4.76 mmol), and Et<sub>3</sub>N (0.66 g, 6.49 mmol) in CH<sub>2</sub>Cl<sub>2</sub> (10.0 mL). The mixture was stirred at rt for 2 h and concentrated in vacuo. Purification by flash chromatography (80/20 Hexane/EtOAc) afforded 1.56 g (98%) of the target compound as a colorless oil. <sup>1</sup>H-NMR (CDCl<sub>3</sub>, 400 MHz): 3.85 (s, 3H, CH<sub>3</sub>), 3.88 (s, 3H, CH<sub>3</sub>), 3.90 (s, 3H, CH<sub>3</sub>), 6.81–6.88 (m, 2H, Ar-H), 6.96 (dd, J = 3.1, 8.8 Hz, 1H, Ar-H), 7.98 (t, J = 8.3 Hz, 1H, Ar-H), 7.58 (d, J = 3.1 Hz, 1H, Ar-H), 7.60 (d, J = 8.8 Hz, 1H, Ar-H); <sup>13</sup>C-NMR (CDCl<sub>3</sub>, 100 MHz): 55.7, 56.1, 60.9, 110.5, 112.6, 115.0, 116.9, 119.6, 123.5, 131.8, 135.3, 141.2, 144.0, 153.8, 158.6, 164.0.

### 3,4,8-Trimethoxy-6H-benzo[*c*]chromen-6-one (**r**)

To a solution of 2,3-dimethoxyphenyl 2-bromo-5-methoxybenzoate (**p**, 1.00 g, 2.72 mmol) in dry DMF (10.0 mL), NaOAc (0.446 g, 5.47 mmol), Pd(OAc)<sub>2</sub> (0.061, 0.27 mmol), and

tricyclohexylphosphine tetrafluoroborate (0.300 g, 0.81 mmol) were added. The mixture was degassed and then refluxed under nitrogen for 3 days. The reaction mixture was cooled to rt, and then diluted with diethyl ether and filtered through Celite to remove the catalyst. The solvent was removed under vacuum to give 1.1 g of a dark oil. Crystallization from MeOH afforded 0.160 g of the target compound as a white solid. m.p. = 187–189 °C; <sup>1</sup>H-NMR (CDCl<sub>3</sub>, 400 MHz): 3.91 (s, 3H, CH<sub>3</sub>), 3.94 (s, 3H, CH<sub>3</sub>), 4.00 (s, 3H, CH<sub>3</sub>), 6.90 (d, J = 8.9 Hz, 1H, Ar-H), 7.33 (dd, J = 2.8, 8.9 Hz, 1H, Ar-H), 7.62 (d, J = 8.9 Hz, 1H, Ar-H), 7.74 (d, J = 2.8 Hz, 1H, Ar-H), 7.89 (d, J = 8.9 Hz, 1H, Ar-H); <sup>13</sup>C-NMR (CDCl<sub>3</sub>, 100 MHz): 55.7, 56.3, 61.5, 108.6, 111.0, 112.7, 116.7, 120.9, 123.0, 124.4, 128.6, 136.8, 144.6, 153.4, 159.3, 160.9. 3,4,8-Trihydroxy-6H-benzo[c]chromen-6-one (15)

The compound was synthesized according to the literature procedure [31]. To a solution of 3,4,8-trimethoxy-6H-benzo[c]chromen-6-one (r, 0.080 g, 0.28 mmol) in CH<sub>2</sub>Cl<sub>2</sub> (10.0 mL), BBr<sub>3</sub> in CH<sub>2</sub>Cl<sub>2</sub> (1.0 M, 1.67 mmol) was added dropwise at 0 °C. The solution was stirred at rt for 12 h. Water (20.0 mL) was added to quench the reaction and the aqueous layer was extracted with EtOAc (3 × 20 mL). The organic phase was dried (Na<sub>2</sub>SO<sub>4</sub>), filtered, and concentrated in vacuo to give a white powder. The solid obtained was triturated in Et<sub>2</sub>O and filtered to afford 0.060 g (88%) of the target compound as yellow solid. m.p. = 341–343 °C; <sup>1</sup>H-NMR (CD<sub>3</sub>OD, 400 MHz): 6.80 (d, J = 8.7 Hz, 1H, Ar-H), 7.28 (dd, J = 2.7, 8.7 Hz, 1H, Ar-H), 7.42 (d, J = 8.7 Hz, 1H, Ar-H), 7.59 (d, J = 2.7 Hz, 1H, Ar-H), 7.97 (d, J = 8.7 Hz, 1H, Ar-H); <sup>13</sup>C-NMR (CD<sub>3</sub>OD, 100 MHz): 111.1, 111.9, 112.1, 113.4, 120.1, 123.2, 123.8, 128.1, 132.5, 138.8, 146.4, 157.0, 161.6; HRMS: found M-H: m/z 243.0307, calculated value for C<sub>13</sub>H<sub>7</sub>O<sub>5</sub>−: 243.0299 (delta: −3.3 ppm).

## 2.2. Kinase Assay

The assay was performed externally at BPS Bioscience (San Diego, CA, USA). Pyruvate kinase (PKL and PKR) reactions were conducted in triplicate at rt for 30 min in a 25 μL mixture containing 50 mM tris, pH 7.4, 10 mM MgCl<sub>2</sub>, 100 mM KCl, 0.05% Tween, 0.1 mM ADP, 0.125 mM PEP, pyruvate kinase (see Supplementary Materials) and the test compounds (see Supplementary Materials). The final DMSO concentration in the reaction was 1% v/v. After enzymatic reactions, 25 μL of Kinase-Glo Max reagent was added to each well and luminescence was measured using a BioTek Synergy<sup>TM</sup> 2 microplate reader. The Kinase-Glo Max luminescence assay kit measures PK activity by quantitating the amount of ATP produced following a PK reaction. Enzyme activity assays were performed in triplicate at each concentration. The luminescence data were analyzed using GraphPad Prism. In the absence of the compound, the intensity (C<sub>e</sub>) in each data set was defined as 100% activity. In the absence of the enzyme, the intensity (C<sub>0</sub>) in each data set was defined as 0% activity. The percentage activity in the presence of each compound was calculated according to the following equation: % activity = (C − C<sub>0</sub>)/(C<sub>e</sub> − C<sub>0</sub>), where C is the luminescence in the presence of the compound.

## 2.3. Molecular Modelling

### 2.3.1. Homology Modelling

A homology model of inactive PKL was constructed for induced-fit docking (IFD) using the reported crystal structure of PKM2. PKM2 has been crystallized in both an active R-state and an inactive T-state, while no crystal structure of PKL in the inactive state is available [32–34]. For this reason and due to the high degree of homology, the 3D structure of inactive PKM2 (PDBID: 6GG4) was used as the template structure for the homology modelling of the inactive PKL tetramer [32]. The PKL protein sequence was retrieved from Uniprot (entry: P30613). The homology model of inactive PKL was built using the StructurePrediction panel in Schrödinger Suite (Schrödinger, LLC, New York, NY, USA) [35]. The ClustalW method was used to align the target and template sequences in Prime. The energy-based method was selected for model building, and homo-multimer was selected as the multi-template model type.



### 2.3.2. Induced Fit Docking

IFD was performed to identify the potential interactions of the compounds with the protein [36]. All compounds were prepared using the LigPrep module, and the protein was prepared using the Protein Preparation Wizard in Schrödinger. The compounds were docked to the rigid protein using Glide with a protein van der Waals radii scaling of 0.5, and ligand van der Waals scaling of 0.5. The resulting top 20 docking poses were used to sample the binding pocket plasticity. Residues within 5 Å of the 20 ligand poses were subject to side chain optimization, with the remainder of the residues held fixed. Therefore, the flexibility of the protein was considered for the forward redocking stage. The parameters for the redocking were all set to default.

### 2.3.3. Prime-MMGBSA Energy Calculations

The binding free energy of the protein–ligand complexes was calculated by the Prime MM-GBSA method. The best IFD docking poses of each protein–ligand complex were used for this calculation. The following equation was used to determine the binding free energies  $\Delta G_{\text{bind}}$ :

$$\Delta G_{\text{bind}} = G_{\text{complex}} - (G_{\text{protein}} + G_{\text{ligand}}) \quad (1)$$

where  $G = E_{\text{MM}} + G_{\text{SGB}} + G_{\text{NP}}$ .  $E_{\text{MM}}$  is the molecular mechanism energies,  $G_{\text{SGB}}$  is SGB solvation energy for polar solvation, and  $G_{\text{NP}}$  is a nonpolar solvation energy.

## 3. Results

### 3.1. Chemistry

Compounds **1**, **2**, **3**, **5**, **7**, **11**, and **12** were commercially available and were purchased from the corresponding vendor. Some of the target compounds (**4**, **8**, **9**, **10**, and **15**) were reported previously in the chemical literature; their synthesis was replicated here, and the molecules were isolated and characterized accordingly [24,29–31]. The other compounds **6**, **13**, and **14** were synthesized in-house.

### 3.2. Initial Screening Results

Initial screening was performed on a selected library of polyphenols, which identified three compounds possessing an inhibitory effect on PKL (Figure 1A). EA (**1**) was the most effective with an  $\text{IC}_{50}$  of 0.032  $\mu\text{M}$ . Table 1 reports the  $\text{IC}_{50}$  values for all compounds.

**Table 1.** In vitro Pyruvate Kinase assay.

Compound	PKL $\text{IC}_{50}$	PKR $\text{IC}_{50}$	PKM1 $\text{IC}_{50}$	PKM2 $\text{IC}_{50}$
<b>1</b>	0.032 $\mu\text{M}$	4.7 $\mu\text{M}$	81 $\mu\text{M}$	0.07 $\mu\text{M}$ <sup>a</sup>
<b>2</b>	12 $\mu\text{M}$	>100 $\mu\text{M}$	N.D.	N.D.
<b>3</b>	2.1 $\mu\text{M}$	7.4 $\mu\text{M}$	N.D.	N.D.
<b>4</b>	0.025 $\mu\text{M}$	0.49 $\mu\text{M}$	8 $\mu\text{M}$	>100 $\mu\text{M}$
<b>5</b>	0.028 $\mu\text{M}$	1.27 $\mu\text{M}$	36 $\mu\text{M}$	0.03 $\mu\text{M}$ <sup>a</sup>
<b>6</b>	Inactive <sup>b</sup>	Inactive <sup>b</sup>	N.D.	N.D.
<b>7</b>	Inactive <sup>b</sup>	Inactive <sup>b</sup>	N.D.	N.D.
<b>8</b>	3.5 $\mu\text{M}$	12 $\mu\text{M}$	N.D.	N.D.
<b>9</b>	2.4 $\mu\text{M}$	5.1 $\mu\text{M}$	N.D.	N.D.
<b>10</b>	0.41 $\mu\text{M}$	2.6 $\mu\text{M}$	N.D.	N.D.
<b>11</b>	Inactive <sup>b</sup>	Inactive <sup>b</sup>	N.D.	N.D.
<b>12</b>	Inactive <sup>b</sup>	Inactive <sup>b</sup>	N.D.	N.D.
<b>13</b>	3.9 $\mu\text{M}$	43 $\mu\text{M}$	N.D.	N.D.
<b>14</b>	2.1 $\mu\text{M}$	68 $\mu\text{M}$	N.D.	N.D.
<b>15</b>	1.7 $\mu\text{M}$	>100 $\mu\text{M}$	N.D.	N.D.
<b>FBP</b> <sup>*</sup>	0.02 $\mu\text{M}$ <sup>a</sup>	0.01 $\mu\text{M}$ <sup>a</sup>	Inactive	0.05 $\mu\text{M}$ <sup>a</sup>

<sup>a</sup> The compound behaves as an activator. The value refers to  $\text{EC}_{50}$ ; <sup>b</sup> compounds with less than 30% inhibition at 10  $\mu\text{M}$  were considered inactive. \*FBP = Fructose-1,6-biphosphate.

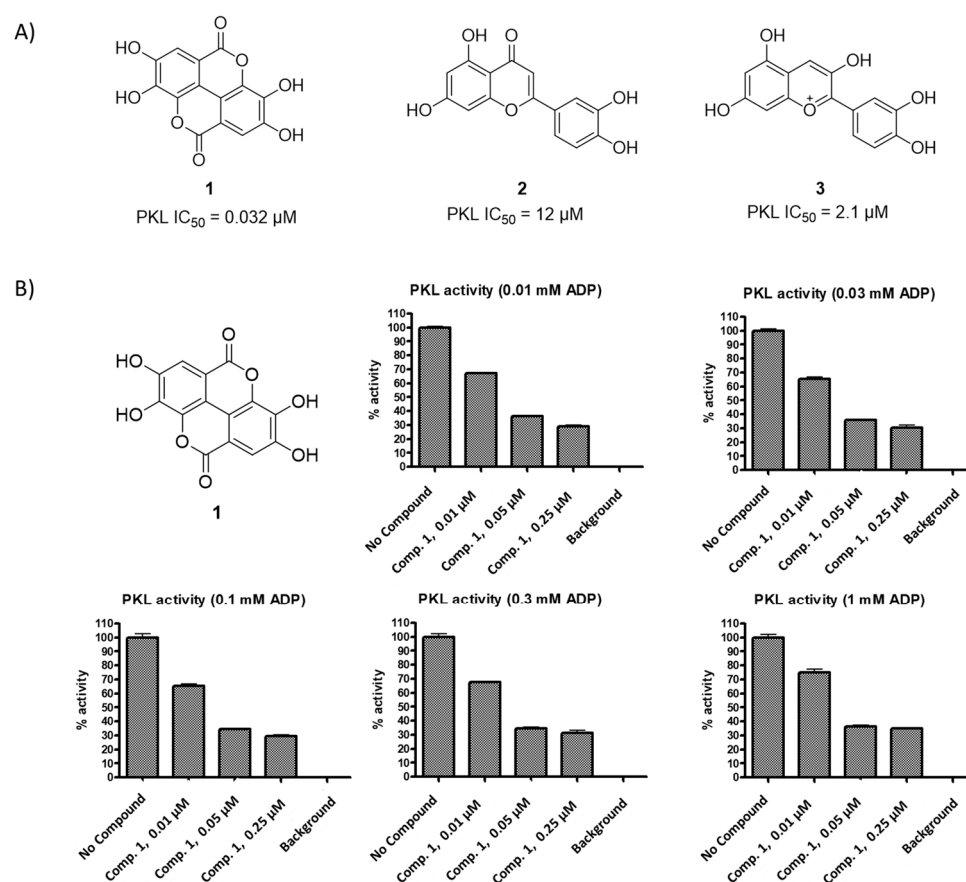


**Figure 1.** (A) Polyphenols exhibiting PKL inhibition. Ellagic acid (EA, 1), luteolin (2), cyanidin (3). (B) Inhibition of PKL by compound 1 at different concentrations of the substrate ADP.

Compound 1 was then evaluated against the other PK isoforms, showing a very good selectivity profile (Table 1). This behavior implied non-competitive inhibition, and in order to test this, we evaluated the activity of compound 1 in the presence of different concentrations of ADP (Figure 1B). The observed activity was independent of substrate concentration, confirming that 1 is a non-competitive allosteric inhibitor. EA possesses exceptional pharmacological properties against liver toxicity and disease, and it has been successfully employed in the past as a lead compound for the development of a new class of CK2 inhibitors [37,38].

### 3.3. Deconstruction of EA and Its Metabolites

EA is a reasonable starting point for the development of potent and selective PKL inhibitors. EA has a complex structure, is symmetrical in nature, and has unfavorable physicochemical properties. Therefore, rather than investigating simple modifications, we immediately applied the “deconstruction” approach to EA (Figure 2). This strategy involves simplifying the structure step-by-step to identify the elements of the molecule required for PKL activity. We decided to focus our study on the number of rings in the molecule. Firstly, one carbonyl group was omitted, partially removing the C-ring, which resulted in urolithin M5 (Uro M5, 4), a well-known metabolite of EA. Compound 4 showed a similar activity and selectivity to the parent compound (Table 1). Further simplification of 1 yielded another metabolite, urolithin D (Uro D, 5). Again, the compound retained the activity and most of the selectivity of the lead molecule (Table 1). Removal of the C- and D-rings produced the inactive isochromenone 6.

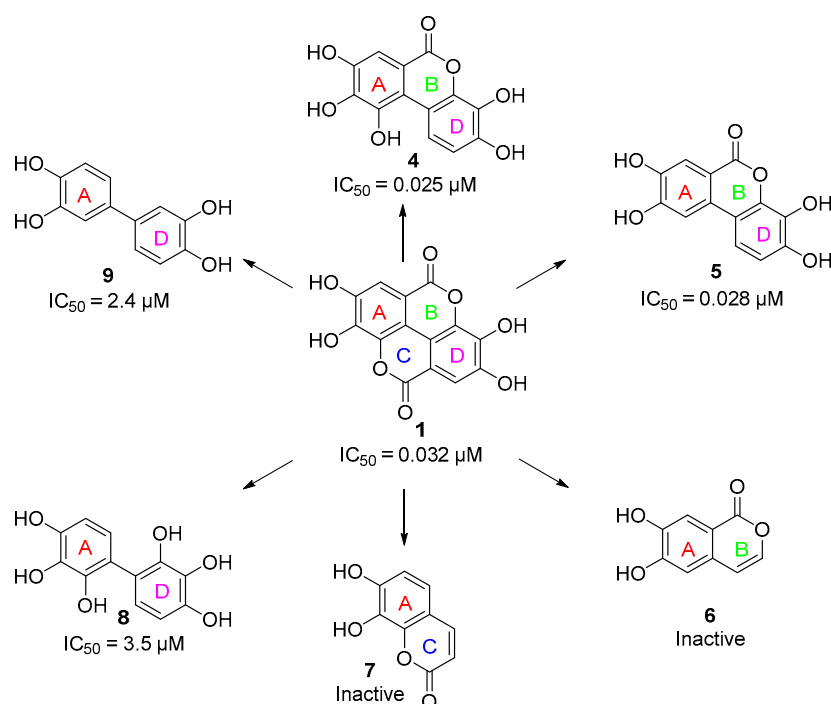


**Figure 2.** Deconstruction of EA and corresponding  $IC_{50}$  vs. PKL.

In terms of the structure–activity relationship, the common features of all active ligands tested in this study were the two aromatic rings and the hydroxyl groups. The lactone moiety seems to play an important but not crucial role. Since the two most active compounds, 4 and 5, are generated *in vivo* from EA metabolism, we decided to test all its possible metabolites. It is well known that EA is gradually metabolized in the intestine to produce urolithin (Uro) M5, Uro D, Uro C, and finally Uro A and Uro B (Figure 3) [38]. All these compounds share the same three-ring system, but they have a different hydroxyl substitution pattern. The removal of a hydroxyl group from 5 produces Uro C (10), which retains some level of activity that is nonetheless reduced by approximately one order of magnitude. Deletion of an additional hydroxyl group, to give Uro A (11), proved to be detrimental for the activity since no inhibition was observed, and similarly for the monohydroxyl compound Uro B (12).

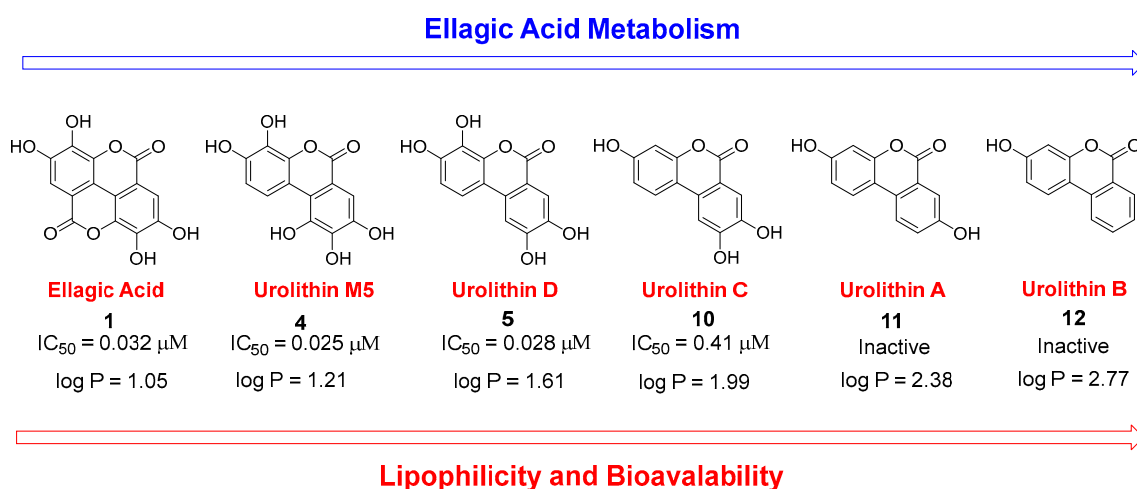


**Figure 3.** EA metabolites and corresponding  $IC_{50}$  vs. PKL.

These data suggest that the hydroxyl groups at position 4 and especially those at position 9 play a critical role in the binding. However, we decided to further investigate

which of the hydroxyl groups of Uro D are required for binding (Figure 4). The deletion of the 3-hydroxyl moiety to give **13** caused a hundred-fold reduction in activity. Removal of the 8-hydroxyl group of **5** gave 8-des-OH Uro D (**14**), and removal of the 9-hydroxyl group gave 9-des-OH Uro D (**15**). Both agents had dramatically reduced inhibitory activity. Evidently, all the hydroxyl groups of Uro D modulate the potency, but the very presence of hydroxyl groups per se is not a requirement for the desired activity.

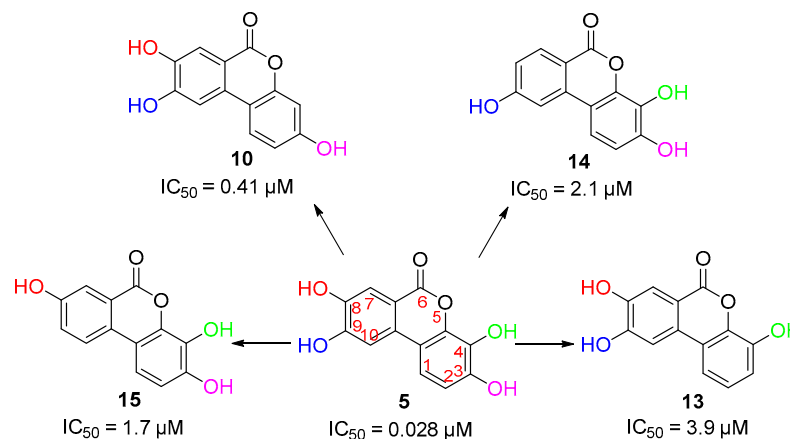


**Figure 4.** Urolithin C positional isomers and corresponding  $IC_{50}$  vs. PKL.

### 3.4. Molecular Modelling Studies

To further understand the binding mode, binding site, and binding energy between EA derivatives and PKL, molecular modelling studies were performed. Initially, we attempted to rationalize our data by docking our active molecules into the PKL crystal structure (PDB ID: 3U2Z). Induced-fit docking was performed to search for potential interactions of the compounds with PKL. This setup takes into account the protein flexibility, which provides a higher degree of accuracy. As shown in Figure 5A, four possible binding pockets have been previously reported in the PKL structure for small molecules: FBP, PEP, ADP, and Phe binding pockets [39]. As such, we speculated that these new inhibitors might bind to one of these binding pockets. However, the ADP binding site was immediately disqualified from the docking study, since we demonstrated unequivocally that **1** is a non-competitive inhibitor.

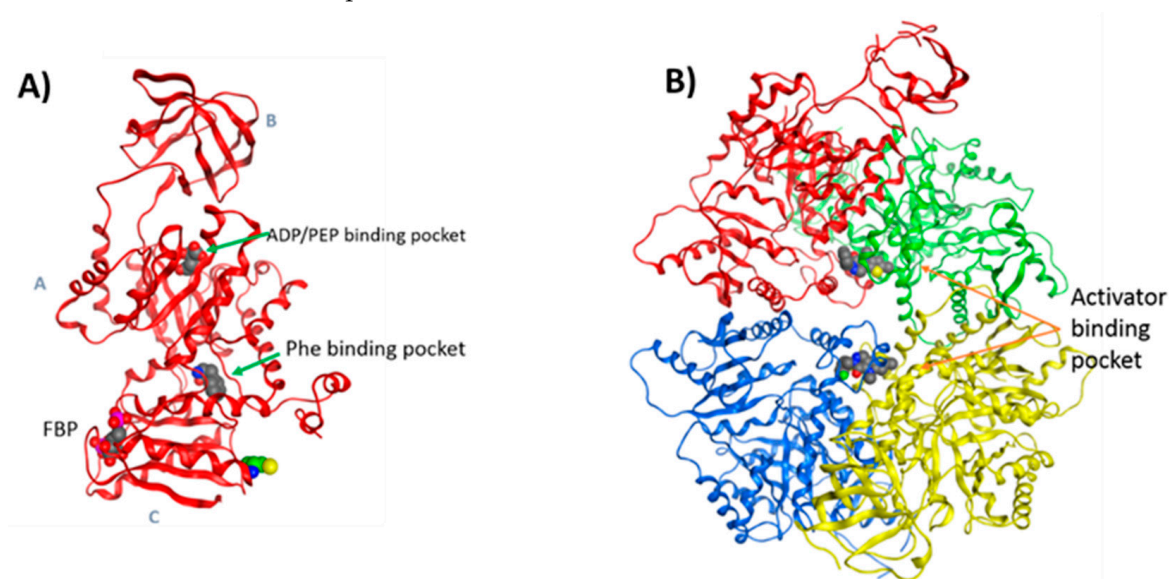


**Figure 5.** (A) Monomeric structure of PKL with different binding sites illustrated. (B) PKM2 active tetramer structure with activator binding (PDB ID: 3U2Z) [36].

Moreover, a detailed analysis of the crystal structure and the literature revealed an additional possible binding site. Compound **1** behaves as a weak activator for PKM2, and has a very planar structure. Recently, a class of PKM2 activators with the same planarity as compound **1** were reported to bind to the inter-monomer interface of the active PKM2 tetramer (Figures 5B and 6A). These PKM2 activators bind between two phenylalanine residues and form  $\pi$ - $\pi$  interactions at the binding interface, thereby stabilizing the active tetramer (Figure 6A) [40]. For this reason, we hypothesize that EA and its derivatives might bind in the same fashion to the PKL dimer interface, resulting in inhibition rather than activation. Furthermore, compound **1** has been previously crystallized with two proteins, glycogen phosphorylase [41] and human CK2 alpha [42]. When analyzing the binding pockets of these two proteins, we found that **1** has a very similar binding pose in both crystal structures, since it lies between a phenylalanine and a tyrosine residue forming  $\pi$ - $\pi$  interactions (Figure 6B).

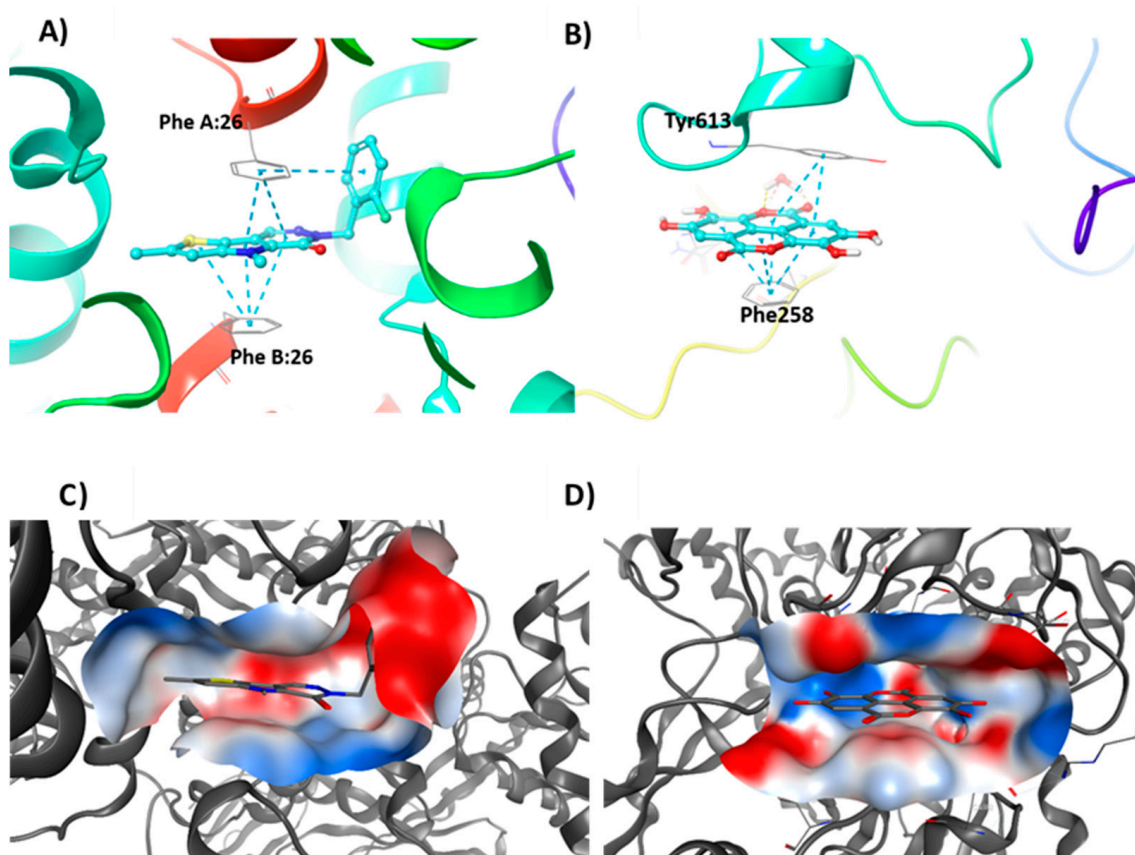


**Figure 6.** (A) Crystal structure of PKM2 activator in its binding site, PDB ID: 3H6O. (B) Crystal structure of compound **1** and glycogen phosphorylase, PDB ID: 4YUA. (C) Electrostatic map of the PKL binding pocket. The backbone is illustrated as a grey ribbon. (D) Electrostatic map of the glycogen phosphorylase binding pocket. The backbone is illustrated as a grey ribbon.

As these binding modes are remarkably close to what was observed in PKM2, we also included this site in the docking study. Therefore, the FBP, PEP, and Phe pockets and the pocket at the binding interface of inactive PKL were selected for IFD to investigate the potential binding interactions of compound **1**. EA was docked into the different binding pockets, and the prime MMGBSA method was used to calculate the relative binding energies ( $\Delta G_{\text{bind}}$ ) of the complex. More negative values of  $\Delta G_{\text{bind}}$  indicate stronger binding. The data obtained (Table 2) showed that compound **1** has a stronger interaction with the binding site located at the tetramer interface of PKL, suggesting that the observed inhibition might be related to the stabilization of the inactive PKL state.

**Table 2.** The binding energies of compound 1 in different binding sites.

Binding Site	$\Delta G_{\text{bind}}$ (kcal/mol) <sup>a</sup>
FBP	−66.56
PEP	−39.51
Phe	−72.11
Inactive tetramer interface	−75.36

$$^a \Delta G_{\text{bind}} = E_{\text{complex}} - (E_{\text{protein}} + E_{\text{ligand}}).$$

The best binding pose of compound 1 in the inactive tetramer interface is shown in Figure 7, and involves two phenylalanine residues from Chain B and E;  $\pi$ – $\pi$  interactions therefore play an important role.

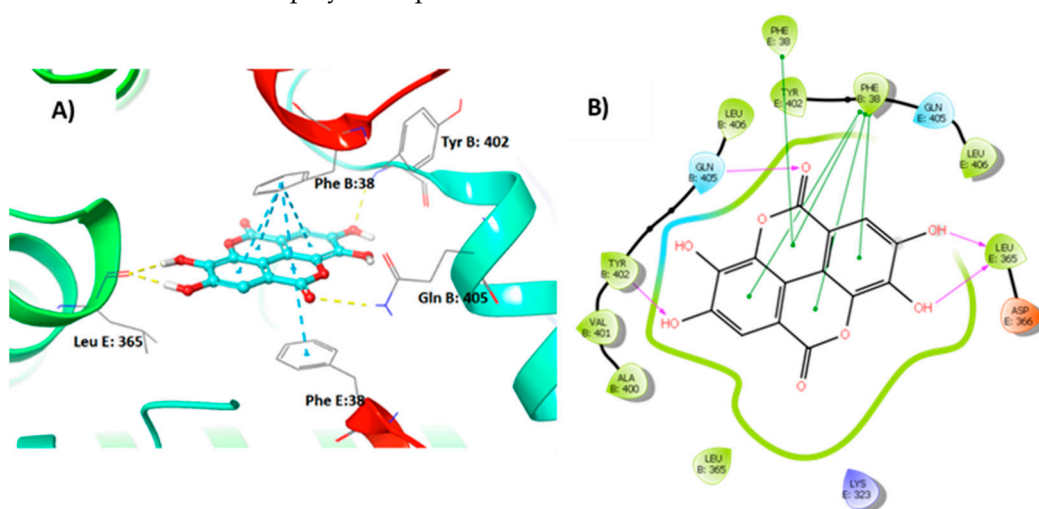


**Figure 7.** Compound 1 interactions with PKL tetramer. (A) 3D structure of the binding pose. (B) 2D structure of the binding pose.

Furthermore, two hydroxyl groups form hydrogen bonds to Leu365 of Chain E on the other side of the compound. The hydroxyl group acts as a hydrogen bond acceptor that interacts with the backbone of Tyr402 of Chain B, and the carbonyl forms a hydrogen bond with Gln405 of Chain B. These data are confirmed by the structure–activity relationship studies performed on the EA derivatives. Moreover, this binding mode could explain not only the non-competitive inhibition shown by 1, but also the good selectivity observed versus PKR, notwithstanding the high homology sequence.

#### 4. Discussion

EA is a polyphenol commonly found in various fruits [43], and it is metabolized in vivo into urolithins, which may mediate its pharmacological effects [44–46]. Several studies have revealed that EA possesses potent biochemical and biological activities, including antioxidative, anti-inflammatory, and neuroprotective effects. EA substantially decreased de novo lipogenesis in adipocytes [47] and hepatocytes [48], and could activate the AMP-activated protein kinase (AMPK) [49]. Urolithins prevented triglyceride synthesis and accumulation, and concomitant downregulation of suppressing fatty acid synthase (FAS) by activating AMPK [50]. Furthermore, EA has also been shown to ameliorate hepatic steatosis by activating AMPK [51]. In this study, EA and its metabolites were identified as potent inhibitors of PKL. As previously reported, PKL upregulation is strongly associated with NAFLD severity [8,9]. Our data suggest that the effect of EA and its metabolites on hepatic steatosis, at least in part, is mediated through inhibition of PKL. Moreover, the structure–activity relationship of these compounds (Figure 8) was investigated using in vitro inhibition assays and molecular docking. The minimum requirements to retain nanomolar activity were (a) 4 hydroxyl groups at positions 3, 4, 8 and 9 on the urolithin core, (b) one lactone moiety (ring b), and (c) the planarity of the structure. Molecular docking

provided valuable insight into the binding interactions of EA and its derivatives. This study provides a new class of non-competitive inhibitors of PKL. We speculate that Uro-D and Uro-C, in particular, could be used as starting points to develop new PKL inhibitors with better drug-like properties. These compounds could be useful in preventing or treating NAFLD. Studies are ongoing to evaluate their effect *in vivo*, and will be published in due course.

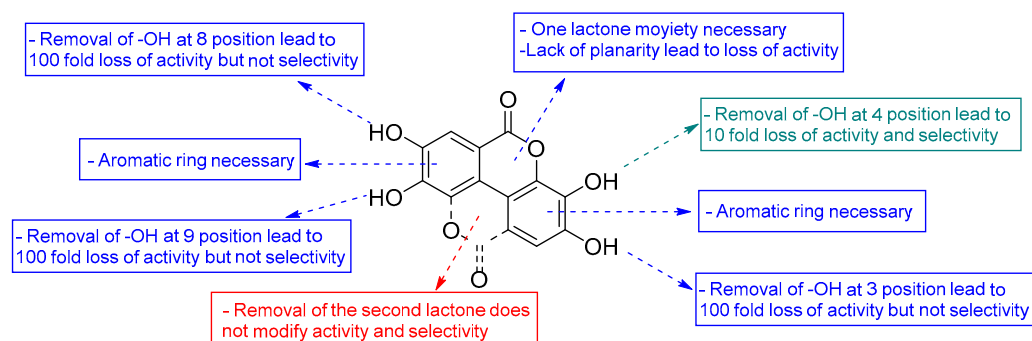


**Figure 8.** SAR study on EA and its derivatives as PKL inhibitors.

**Supplementary Materials:** The following supporting information can be downloaded at: <https://www.mdpi.com/article/10.3390/nu15030577/s1>. Figures of  $^1\text{H}$ - and  $^{13}\text{C}$ -NMR spectra of the synthesized compounds.

**Author Contributions:** Conceptualization, U.M.B., C.G., F.A. and M.G.; methodology, U.M.B., C.G. and F.A.; modelling, C.G.; validation, all; data interpretation, all; original draft preparation, U.M.B. and C.G.; writing—review and editing, all; visualization, U.M.B., C.G. and F.A. All authors have read and agreed to the published version of the manuscript.

**Funding:** The authors acknowledge financial support from the Knut and Alice Wallenberg Foundation for a proof-of-concept grant to J.B., the Swedish Research Council (Grant #: 2019-01049), the Ogonoris Foundation (Grant #: 0063869), ScandiEdge Therapeutics, and the Torsten Söderberg Foundation (Grant #: M105/19).

**Institutional Review Board Statement:** Not applicable.

**Informed Consent Statement:** Not applicable.

**Data Availability Statement:** Data are available in the Supporting Materials.

**Conflicts of Interest:** The authors declare that they have no conflicts of interest.

## References

1. Younossi, Z.; Anstee, Q.M.; Marietti, M.; Hardy, T.; Henry, L.; Eslam, M.; George, J.; Bugianesi, E. Global burden of NAFLD and NASH: Trends, predictions, risk factors and prevention. *Nat. Rev. Gastroenterol. Hepatol.* **2018**, *15*, 11–20. [[CrossRef](#)]
2. Benedict, M.; Zhang, X. Non-alcoholic fatty liver disease: An expanded review. *World J. Hepatol.* **2017**, *9*, 715–732. [[CrossRef](#)]
3. Albhaisi, S.; Sanyal, A. Recent advances in understanding and managing non-alcoholic fatty liver disease. *F1000Research* **2018**, *7*, 720. [[CrossRef](#)]
4. Cohen, J.C.; Horton, J.D.; Hobbs, H.H. Human Fatty Liver Disease: Old Questions and New Insights. *Science* **2011**, *332*, 1519–1523. [[CrossRef](#)] [[PubMed](#)]
5. Chalasani, N.; Younossi, Z.; Lavine, J.E.; Diehl, A.M.; Brunt, E.M.; Cusi, K.; Charlton, M.; Sanyal, A.J. The Diagnosis and Management of Non-alcoholic Fatty Liver Disease: Practice Guideline by the American Gastroenterological Association, American Association for the Study of Liver Diseases, and American College of Gastroenterology. *Gastroenterology* **2012**, *142*, 1592–1609. [[CrossRef](#)] [[PubMed](#)]
6. Friedman, S.L.; Neuschwander-Tetri, B.A.; Rinella, M.; Sanyal, A.J. Mechanisms of NAFLD development and therapeutic strategies. *Nat. Med.* **2018**, *24*, 908–922. [[CrossRef](#)]
7. Lee, S.; Zhang, C.; Liu, Z.; Klevstig, M.; Mukhopadhyay, B.; Bergentall, M.; Cinar, R.; Stahlman, M.; Sikanic, N.; Park, J.K.; et al. Network analyses identify liver-specific targets for treating liver diseases. *Mol. Syst. Biol.* **2017**, *13*, 938. [[CrossRef](#)] [[PubMed](#)]
8. Chella Krishnan, K.; Kurt, Z.; Barrere-Cain, R.; Sabir, S.; Das, A.; Floyd, R.; Vergnes, L.; Zhao, Y.; Che, N.; Charugundla, S.; et al. Integration of Multi-omics Data from Mouse Diversity Panel Highlights Mitochondrial Dysfunction in Non-alcoholic Fatty Liver Disease. *Cell Syst.* **2018**, *6*, 103–115.E7. [[CrossRef](#)] [[PubMed](#)]

9. Mardinoglu, A.; Uhlen, M.; Borén, J. Broad Views of Non-alcoholic Fatty Liver Disease. *Cell Syst.* **2018**, *6*, 7–9. [[CrossRef](#)] [[PubMed](#)]
10. Muirhead, H. Isoenzymes of pyruvate kinase. *Biochem. Soc. Trans.* **1990**, *18*, 193–196. [[CrossRef](#)]
11. Cardenas, J.M.; Dyson, R.D. Mammalian pyruvate kinase hybrid isozymes: Tissue distribution and physiological significance. *J. Exp. Zool.* **1978**, *204*, 361–367. [[CrossRef](#)] [[PubMed](#)]
12. Imamura, K.; Tanaka, T. Multimolecular Forms of Pyruvate Kinase from Rat and Other Mammalian Tissues I. Electrophoretic Studies. *J. Biochem.* **1972**, *71*, 1043–1051. [[CrossRef](#)] [[PubMed](#)]
13. Strandholm, J.J.; Dyson, R.D.; Cardenas, J.M. Bovine pyruvate kinase isozymes and hybrid isozymes: Electrophoretic studies and tissue distribution. *Arch. Biochem. Biophys.* **1976**, *173*, 125–131. [[CrossRef](#)] [[PubMed](#)]
14. Yamada, K.; Noguchi, T. Nutrient and hormonal regulation of pyruvate kinase gene expression. *Biochem. J.* **1999**, *337*, 1–11. [[CrossRef](#)]
15. Aslan, E.; Guler, C.; Adem, S. In vitro effects of some flavonoids and phenolic acids on human pyruvate kinase isoenzyme M2. *J. Enzyme Inhib. Med. Chem.* **2016**, *31*, 314–317. [[CrossRef](#)]
16. Yang, P.; Ding, G.-B.; Liu, W.; Fu, R.; Sajid, A.; Li, Z. Tannic acid directly targets pyruvate kinase isoenzyme M2 to attenuate colon cancer cell proliferation. *Food Funct.* **2018**, *9*, 5547–5559. [[CrossRef](#)]
17. Adem, S.; Aslan, A.; Ahmed, I.; Krohn, K.; Guler, C.; Comaklı, V.; Demirdag, R.; Kuzu, M. Inhibitory and Activating Effects of Some Flavonoid Derivatives on Human Pyruvate Kinase Isoenzyme M2. *Arch. Pharm.* **2015**, *349*, 132–136. [[CrossRef](#)]
18. Rodriguez-Ramiro, I.; Vauzour, D.; Miniñane, A.M. Polyphenols and non-alcoholic fatty liver disease: Impact and mechanisms. *Proc. Nutr. Soc.* **2016**, *75*, 47–60. [[CrossRef](#)]
19. Ludovico, A.; Natasa, M.; Francesco, L.; Luigi, B.; Antonino De, L. Polyphenols treatment in patients with nonalcoholic fatty liver disease. *J. Transl. Int. Med.* **2017**, *5*, 144–147.
20. Li, S.; Tan, H.Y.; Wang, N.; Cheung, F.; Hong, M.; Feng, Y. The Potential and Action Mechanism of Polyphenols in the Treatment of Liver Diseases. *Oxid. Med. Cell. Longev.* **2018**, *2018*, 25. [[CrossRef](#)]
21. Van De Wier, B.; Koek, G.H.; Bast, A.; Haenen, G.R.M.M. The potential of flavonoids in the treatment of non-alcoholic fatty liver disease. *Crit. Rev. Food Sci. Nutr.* **2017**, *57*, 834–855. [[CrossRef](#)] [[PubMed](#)]
22. Sharifi-Rad, J.; Quispe, C.; Castillo, C.M.S.; Caroca, R.; Lazo-Vélez, M.A.; Antonyak, H.; Polishchuk, A.; Lysiuk, R.; Oliinyk, P.; De Masi, L.; et al. Ellagic Acid: A Review on Its Natural Sources, Chemical Stability, and Therapeutic Potential. *Oxid. Med. Cell. Longev.* **2022**, *2022*, 3848084. [[CrossRef](#)] [[PubMed](#)]
23. Cozza, G.; Bonvini, P.; Zorzi, E.; Poletto, G.; Pagano, M.A.; Sarno, S.; Donella-Deana, A.; Zagotto, G.; Rosolen, A.; Pinna, L.A.; et al. Identification of ellagic acid as potent inhibitor of protein kinase CK2: A successful example of a virtual screening application. *J. Med. Chem.* **2006**, *49*, 2363–2366. [[CrossRef](#)] [[PubMed](#)]
24. Cozza, G.; Gianoncelli, A.; Bonvini, P.; Zorzi, E.; Pasquale, R.; Rosolen, A.; Pinna, L.A.; Meggio, F.; Zagotto, G.; Moro, S. Urolithin as a Converging Scaffold Linking Ellagic acid and Coumarin Analogues: Design of Potent Protein Kinase CK2 Inhibitors. *ChemMedChem* **2011**, *6*, 2273–2286. [[CrossRef](#)]
25. Dasaradhan, C.; Kumar, Y.S.; Prabakaran, K.; Khan, F.-R.N.; Jeong, E.D.; Chung, E.H. Efficient and convenient copper-free Pd(OAc)<sub>2</sub>/Ruphos-catalyzed Sonogashira coupling in the preparation of corfin analogues. *Tetrahedron Lett.* **2015**, *56*, 784–788. [[CrossRef](#)]
26. Greenberg, J.A.; Sammakia, T. The Conversion of tert-Butyl Esters to Acid Chlorides Using Thionyl Chloride. *J. Org. Chem.* **2017**, *82*, 3245–3251. [[CrossRef](#)]
27. Toure, M.; Jaime-Figueroa, S.; Burslem, G.M.; Crews, C.M. Expedient Synthesis of Isoquinolones and Isocoumarins with a Vinyl Borane as an Acetylene Equivalent. *Eur. J. Org. Chem.* **2016**, *2016*, 4171–4175. [[CrossRef](#)]
28. Battisti, U.M.; Jozwiak, K.; Cannazza, G.; Puia, G.; Stocca, G.; Braghiroli, D.; Parenti, C.; Brasili, L.; Carrozzo, M.M.; Citti, C.; et al. 5-Arylbenzothiadiazine Type Compounds as Positive Allosteric Modulators of AMPA/Kainate Receptors. *ACS Med. Chem. Lett.* **2012**, *3*, 25–29. [[CrossRef](#)]
29. Liang, Y.-F.; Li, X.; Wang, X.; Zou, M.; Tang, C.; Liang, Y.; Song, S.; Jiao, N. Conversion of Simple Cyclohexanones into Catechols. *J. Am. Chem. Soc.* **2016**, *138*, 12271–12277. [[CrossRef](#)]
30. Goins, C.M.; Dajnowicz, S.; Thanna, S.; Sucheck, S.J.; Parks, J.M.; Ronning, D.R. Exploring Covalent Allosteric Inhibition of Antigen 85C from Mycobacterium tuberculosis by Ebselen Derivatives. *ACS Infect. Dis.* **2017**, *3*, 378–387. [[CrossRef](#)]
31. Weidner-Wells, M.A.; Altom, J.; Fernandez, J.; Fraga-Spano, S.A.; Hilliard, J.; Ohemeng, K.; Barrett, J.F. DNA gyrase inhibitory activity of ellagic acid derivatives. *Bioorg. Med. Chem. Lett.* **1998**, *8*, 97–100. [[CrossRef](#)] [[PubMed](#)]
32. Yuan, M.; McNae, I.W.; Chen, Y.; Blackburn, E.A.; Wear, M.A.; Michels, P.A.M.; Fothergill-Gilmore, L.A.; Hupp, T.; Walkinshaw, M.D. An allostatic mechanism for M2 pyruvate kinase as an amino-acid sensor. *Biochem. J.* **2018**, *475*, 1821–1837. [[CrossRef](#)] [[PubMed](#)]
33. Holyoak, T.; Zhang, B.; Deng, J.; Tang, Q.; Prasanna, C.B.; Fenton, A.W. Energetic coupling between an oxidizable cysteine and the phosphorylatable N-terminus of human liver pyruvate kinase. *Biochem.* **2013**, *52*, 466–476. [[CrossRef](#)] [[PubMed](#)]
34. Morgan, H.P.; O'Reilly, F.J.; Wear, M.A.; O'Neill, J.R.; Fothergill-Gilmore, L.A.; Hupp, T.; Walkinshaw, M.D. M2 pyruvate kinase provides a mechanism for nutrient sensing and regulation of cell proliferation. *Proc. Natl. Acad. Sci. USA* **2013**, *110*, 5881–5886. [[CrossRef](#)]



35. Jacobson, M.P.; Friesner, R.A.; Xiang, Z.; Honig, B. On the Role of the Crystal Environment in Determining Protein Side-chain Conformations. *J. Mol. Biol.* **2002**, *320*, 597–608. [[CrossRef](#)]
36. Sherman, W.; Day, T.; Jacobson, M.P.; Friesner, R.A.; Farid, R. Novel Procedure for Modeling Ligand/Receptor Induced Fit Effects. *J. Med. Chem.* **2006**, *49*, 534–553. [[CrossRef](#)]
37. García-Niño, W.R.; Zazueta, C. Ellagic acid: Pharmacological activities and molecular mechanisms involved in liver protection. *Pharmacol. Res.* **2015**, *97*, 84–103. [[CrossRef](#)]
38. Cozza, G. The Development of CK2 Inhibitors: From Traditional Pharmacology to in Silico Rational Drug Design. *Pharmaceuticals* **2017**, *10*, 26. [[CrossRef](#)]
39. Tang, Q.; Villar, M.T.; Artigues, A.; Thyfault, J.P.; Apte, U.; Zhu, H.; Peterson, K.R.; Fenton, A.W. Mutational mimics of allosteric effectors: A genome editing design to validate allosteric drug targets. *Sci. Rep.* **2019**, *9*, 9031. [[CrossRef](#)]
40. Anastasiou, D.; Yu, Y.; Israelsen, W.J.; Jiang, J.-K.; Boxer, M.B.; Hong, B.S.; Tempel, W.; Dimov, S.; Shen, M.; Jha, A.; et al. Pyruvate kinase M2 activators promote tetramer formation and suppress tumorigenesis. *Nat. Chem. Biol.* **2012**, *8*, 839. [[CrossRef](#)]
41. Kyriakis, E.; Stravodimos, G.A.; Kantsadi, A.L.; Chatzileontiadou, D.S.M.; Skamnaki, V.T.; Leonidas, D.D. Natural flavonoids as antidiabetic agents. The binding of gallic and ellagic acids to glycogen phosphorylase b. *FEBS Lett.* **2015**, *589*, 1787–1794. [[CrossRef](#)]
42. Sekiguchi, Y.; Nakaniwa, T.; Kinoshita, T.; Nakanishi, I.; Kitaura, K.; Hirasawa, A.; Tsujimoto, G.; Tada, T. Structural insight into human CK2 $\alpha$  in complex with the potent inhibitor ellagic acid. *Bioorg. Med. Chem. Lett.* **2009**, *19*, 2920–2923. [[CrossRef](#)] [[PubMed](#)]
43. Evtugin, D.D.; Magina, S.; Evtugin, D.V. Recent advances in the production and applications of ellagic acid and its derivatives. A review. *Molecules* **2020**, *25*, 2745. [[CrossRef](#)]
44. Seo, C.S.; Jeong, S.J.; Yoo, S.R.; Lee, N.R.; Shin, H.K. Quantitative analysis and in vitro anti-inflammatory effects of gallic acid, ellagic acid, and quercetin from radix sanguisorbae. *Pharmacogn Mag.* **2016**, *12*, 104–108. [[CrossRef](#)]
45. Polce, S.A.; Burke, C.; França, L.M.; Kramer, B.; de Andrade Paes, A.M.; Carrillo-Sepulveda, M.A. Ellagic acid alleviates hepatic oxidative stress and insulin resistance in diabetic female rats. *Nutrients* **2018**, *10*, 531. [[CrossRef](#)] [[PubMed](#)]
46. Zhu, H.; Yan, Y.; Jiang, Y.; Meng, X. Ellagic Acid and Its Anti-Aging Effects on Central Nervous System. *Int. J. Mol. Sci.* **2022**, *23*, 10937. [[CrossRef](#)] [[PubMed](#)]
47. Okla, M.; Kang, I.; Kim, D.M.; Gourineni, V.; Shay, N.; Gu, L.; Chung, S. Ellagic acid modulates lipid accumulation in primary human adipocytes and human hepatoma Huh7 cells via discrete mechanisms. *J. Nutr. Biochem.* **2015**, *26*, 82–90. [[CrossRef](#)]
48. Zhang, C.; Hu, J.; Sheng, L.; Yuan, M.; Wu, Y.; Chen, L.; Wang, G.; Qiu, Z. Ellagic acid ameliorates AKT-driven hepatic steatosis in mice by suppressing de novo lipogenesis via the AKT/SREBP-1/FASN pathway. *Food Funct.* **2019**, *10*, 3410–3420. [[CrossRef](#)] [[PubMed](#)]
49. Poulouse, N.; Vishnu Prasad, C.N.; Nidhina Haridas, P.A.; Anilkumar, G. Ellagic Acid Stimulates Glucose Transport in Adipocytes and Muscles through AMPK Mediated Pathway. *J. Diabetes Metab.* **2011**, *2*, 149. [[CrossRef](#)]
50. Kang, I.; Kim, Y.; Tomás-Barberán, F.A.; Espín, J.C.; Chung, S. Urolithin A, C, and D, but not iso-urolithin A and urolithin B, attenuate triglyceride accumulation in human cultures of adipocytes and hepatocytes. *Mol. Nutr. Food Res.* **2016**, *60*, 1129–1138. [[CrossRef](#)]
51. ALTamimi, J.Z.; Alshammari, G.M.; AlFaris, N.A.; Alagal, R.I.; Aljabryn, D.H.; Albekairi, N.A.; Alkhateeb, M.A.; Yahya, M.A. Ellagic acid protects against non-alcoholic fatty liver disease in streptozotocin-diabetic rats by activating AMPK. *Pharm. Biol.* **2022**, *60*, 25–37. [[CrossRef](#)] [[PubMed](#)]

**Disclaimer/Publisher’s Note:** The statements, opinions and data contained in all publications are solely those of the individual author(s) and contributor(s) and not of MDPI and/or the editor(s). MDPI and/or the editor(s) disclaim responsibility for any injury to people or property resulting from any ideas, methods, instructions or products referred to in the content.